N93-30434

DESIGN AND MANUFACTURING CONCEPTS FOR THERMOPLASTIC STRUCTURES

Michael P. Renieri, Steven J. Burpo,
and Lance M. Roundy

McDonnell Aircraft Company
St. Louis, Missouri

SUMMARY

Results to date on the application of two manufacturing techniques, fiber placement and single diaphragm/coconsolidation, to produce cost-effective, thermoplastic composite (TPC), primary fuselage structure are presented. Applications relative to fuselage upper cover structure indicate potential cost savings relative to conventional approaches. Progress is also presented on efforts concerned with other design details which take advantage of thermoplastic composites such as fastenerless stiffener/frame attachments. In addition, results are presented on the development and verification testing of a composite lug analysis program which incorporates through-the-thickness effects.

INTRODUCTION

A major obstacle to widespread use of high performance composites in primary aircraft structures is the high cost of manufacture and assembly. Under NASA's ACT program, McDonnell Aircraft Company is investigating cost-effective, innovative techniques for the fabrication and joining of primary airframe structure using thermoplastic composite materials. MCAIR is teamed with Douglas Aircraft Company (DAC) under the ACT initiative in a program entitled Innovative Composite Aircraft Primary Structures (ICAPS).

Primary effort on the MCAIR portion of the ICAPS program has concentrated on developments relative to an advanced fighter fuselage section which are applicable to commercial vehicle structure. These include the application of two innovative manufacturing techniques, fiber placement and single diaphragm/ coconsolidation to fabricate fuselage cover panels.

In addition to panel fabrication, elemental specimens are being fabricated and tested to address key design issues associated with the fuselage section such as pull-off strength of fastenerless frame attachment concepts and the performance of thick composite lugs. In support of the lug evaluation, an analytical program has been developed incorporating through- the-thickness effects.

GENERIC FUSELAGE SECTION

The advanced aircraft system selected for the fighter development effort was the Model 4629 ASTOVL design developed by MCAIR under the NASA-Ames sponsored U.S./U.K. ASTOVL Technology Development program. Based on representative

fuselage cross sections of the Model 4629 aircraft, a generic center fuselage structure, Figure 1, was developed as the primary structure demonstration component. While the fuselage structure contains design features particular to advanced ASTOVL aircraft, cost effective fabrication techniques and innovative design concepts developed in this program demonstrate technology related to all emerging aircraft systems.

The generic center fuselage structure contains many challenging structural components:

- o Upper Cover
- o Tank Floor
- o Carry-Thru Bulkhead
- o Closure Bulkhead
- o Keel Webs
- o Frames
- o Inlet Ducts
- o Longerons

An upper fuel cell cover subcomponent was selected for design/analysis, fabrication, and structural testing for Phase A. The cover structure ties the upper longerons and bulkheads of the generic fuselage section together and is a primary load carrying component for flight induced structural and fuel cell loading. The cover must be capable of a 255°F (110°C) operating temperature, have a limited number of fasteners on the outer moldline (OML), and resist hydrodynamic ram loading.

MATERIAL AND PROCESS SELECTIONS

Material

The material chosen was based on temperature requirements, solvent resistance, component design, manufacturing approach, and processing ease. Due to the 255°F design requirement, the baseline thermoplastic material selected was Imperial Chemical Industries' ITX (intermediate temperature crystalline), which has service capability to 300°F. The fiber selected was an intermediate modulus fiber produced by Hercules, IM7. ITX has processing characteristics similar to ICI's APC-2 (PEEK) system which is a mature resin that MCAIR has worked with extensively. In addition, AS4/APC-2 was selected for early forming studies due to availability and to verify analytical predictions for thick composite lugs.

Processes

Manufacturing processes were selected using a concurrent engineering approach. Processes were rated based on innovativeness, cost, risk, supportability, survivability, and weight. Two manufacturing techniques, fiber placement and single diaphragm/coconsolidation, were selected to fabricate subscale fuselage cover panels.

Fiber placement (FP), one of the more promising methods of fabrication, is the in situ consolidation of individual material layers using pressure and heat at the point of contact. This procedure eliminates the autoclave requirement and automates the material deposition process reducing significant cost elements in a typical composite production environment.

Secondly, MCAIR is evaluating a method that uses only a single upper diaphragm to form a skin and hat structure in one step. This process, single diaphragm/ coconsolidation (SDCC), simultaneously consolidates the hat stiffened inner skin plies with the outer skin plies while coconsolidating the two yielding a high quality interface and reducing the number of process steps from three to one.

PRODUCIBILITY ANALYSIS

A producibility analysis was performed to determine the cost-effectiveness of the selected processes versus alternate approaches, Reference 1. Three material systems and five design options were considered for the cover. TPC materials are considered in three approaches: SDCC, fiber placement, and manual lay-up. The other two options include a manual lay-up of toughened bismaleimide (BMI) and a titanium superplastic formed diffusion bonded (SPF/DB) design.

The three approaches for thermoplastic composites include (1) SDCC in which a pressure box is employed to consolidate the outer skin while at the same time forming and consolidating the inner stiffened pan, (2) fiber placement, using a tow placement process over preformed hat stiffeners recessed into a fiber placement tool, and (3) a thermoplastic composite manual lay-up approach with autoclave consolidated unidirectional and comingled material forms. A traditional manual lay-up process was considered for the toughened BMI thermoset composite (TSC) design utilizing rubber mandrels and female tooling to produce a co-cured structure. In addition, the TSC design included stitching of the stiffeners to increase stiffeners-to-skin interface strength. A titanium superplastic formed/diffusion bonded design was the metal option. Diffusion bonding allows the economical creation of high performance hat stiffened skins without fasteners.

The analysis explored the impact of component complexity on producibility and cost. Two levels of complexity were considered. The fuel cell cover under development for this program is a single curved component. A producibility analysis of this generic cover was established to serve as a baseline. A complex, doubly curved version of the cover was also considered since OML fighter skins are typically complex surfaces.

High processing temperatures for thermoplastic composites (750°F, 385°C) impose two major fabrication constraints: (1) flexible rubber mandrels (for hat stiffener tooling) cannot be used since they are unable to survive the processing temperatures and (2) high temperature tooling is required instead of aluminum tooling. The influence of these constraints for both recurring and non-recurring costs was considered. Each fabrication approach listed above was evaluated in order to identify the best technique for both levels of complexity.

Recurring component costs were generated by summing material and labor costs for each step of process plans for each fabrication approach. Labor costs were burdened to include equipment/facilities costs. Non-recurring costs took into account tooling expenses, including any duplicate tooling required to produce the theoretical rate of 85 ship sets per year (600 aircraft total). Cost comparisons for this study were normalized; the least expensive simply curved approach is set equal to one with the cost of other options appropriately ratioed.

The cost study results for both complex and simply curved components showed that the SDCC approach was most cost-effective for the cover due to flat ply collation and short cycle times, Figure 2. TPC fiber placement was the next most cost-effective approach due to automated processing of the skin. Although TPC's are difficult to manually lay-up, this process is less expensive than TSC manual lay-up due in part to stitching requirements for TSC in order to increase hat pull off strength. Titanium SPF/DB and TSC were close in recurring cost due to the labor intensive operations required for these approaches. As expected, the recurring cost of fabricating complex structure was consistently higher than simple structure.

Non-recurring costs (tooling) for the five fabrication approaches showed that duplicate tooling requirements for TSC and TPC manual lay-up increase their respective tooling costs to a level comparable to the other fabrication approaches, Figure 3. Even with duplicate tooling, non-recurring costs for simply curved TSC and TPC are the least expensive options. Five-axis machining requirements for tooling on complex curved manual lay-up TSC and TPC approximately doubles their respective non-recurring costs. Although press forming and fiber placement tooling costs are identical for simply curved applications, a substantial cost increase is incurred in press forming versus fiber placement costs for complex curvature. This increase is attributed to difficult machining requirements (five-axis) for not only the press forming tool but also for the associated pressure box. High temperature matched metal steel tools must be supplied for the titanium SPF/DB approach resulting in the highest tooling costs of any approach.

SUBCOMPONENT DESIGN/ANALYSIS AND STRUCTURAL TESTS

Design loads for the upper cover subcomponent, Figure 4, were developed from maneuvering flight conditions consisting of a 9g symmetric steady-state pull-up (SSPU) for down bending, a -3g steady state pushdown (SSPD) for up bending, and 7.2g rolling pull-out (RPO) for combined vertical and lateral loads. All flight conditions are at sea level and 0.95 Mach. A 22.0 psi (ultimate) fuel pressurization load condition is also included.

Design loads were obtained at a fuselage station in the forward-center fuselage section at the most forward wing shear attach location. A hat stiffened skin of single curvature was sized for these loads. Various laminates were evaluated for static strength and panel stability. A finite element model of the cover was used to examine effects of combined loads and determine static deflections. Panel stability was determined using SS8 Anisotropic Curved Panel Analysis Program, Reference 2.

Two designs were developed for the upper cover. The first design, Figure 5, contains discrete hat stiffeners with a constant thickness skin. The second design, Figure 6, contains a constant thickness Inner Mold Line (IML) pan with a buildup under the stiffener in the OML skin. The first design will be utilized in the FP manufacturing process. The second design will be fabricated using the SDCC.

The laminate stacking sequences for the cover subcomponents represent the minimum necessary to sustain all flight load conditions, buckling constraints and fabrication requirements. Skin buckling occurs at 120% of design limit load, a requirement common in new fighter aircraft designs with composite mold line skins.

Planned structural testing of the subcomponents consists of compression static and fatigue loading. Static tests will be used to compare results of structural tests to analytical predictions, while fatigue tests will determine panel resistance to delamination modes of failure due to repeated loads.

ELEMENT DESIGN/ANALYSIS AND STRUCTURAL TESTS

Two structural areas of particular interest in the fuselage structure were selected for elemental evaluation. These are thick composite lugs and stiffener-to-skin joints.

Lug Elements

A method for predicting the static response of thick, highly loaded, composite lugs has been developed. Composite lugs provide a mechanism for the transfer of concentrated loads from one structural member to another. The most notable examples are lugs that transmit wing loads into bulkheads such as those present on the generic fuselage structures. The geometry of these lugs can vary substantially for different applications, and they may be required to carry in-plane as well as out-of-plane loads. In addition, effects such as pin bending may result in complex stress states through the thickness of a lug, even when it is subject to only in-plane loads.

The wide range of variables associated with this problem necessitates the use of an analytical method that is very flexible, both in the range of geometries and the types of load conditions that it is capable of analyzing. The complex through-the-thickness stress distributions that may develop require that the method also be capable of predicting three-dimensional stress fields. The finite element method is one such approach and was the method used in this development.

Laminated composite aircraft components are typically analyzed using plate elements that are based on classical laminated plate theory. These elements are simple to use since the geometry of the element can be defined in two dimensions, and they account for in-plane and out-of-plane loads. They are, however, restricted to the analysis of thin plates, which limits their usefulness for the analysis of thick lugs. The thin plate derivation permits

only linear variations in the in-plane stresses through the thickness of the lug, and out-of-plane stresses are assumed to be negligible.

At the other extreme, a thick lug can be modeled with three-dimensional solid finite elements. Using the approach, each ply can be modeled (one or more plies through the thickness of each element). These elements allow complete generality in defining the lug geometry and loads and are based on assumed three-dimensional displacement fields. Although models generated with these elements provide accurate results, their use is cumbersome and they require substantial computing resources. They are, therefore, not recommended for the type of parametric study that would be required to optimize a lug design.

The approach taken in this program was a compromise between the two methods described above. A subparametric laminated solid element based on cubic displacement functions was used. This element was developed in Reference 3 to study through-the-thickness stress fields that develop during low velocity impact events.

The geometry of this element is defined by four nodes in the X-Y plane, and the stacking sequence of the laminate under consideration, Figure 7. There are twenty-four degrees of freedom at each node. These degrees of freedom are the translations at the upper and lower surfaces of the laminate in each of the three coordinate directions and the derivatives of these translations with respect to each coordinate.

Using conventional finite element methods, the stiffness matrix for the element is generated by integrating the strain energy density over the volume of the element. The effects of stacking sequence are included by performing this integration numerically over the volume of each discrete ply and summing the results. This approach also allows the average strain in each ply and at each interface to be calculated once the translations and derivatives of the translations have been determined.

To account for pin bending effects, both the lug and the pin are modeled. The generation of these models is relatively simple since the geometry is defined in only two dimensions. The lug/pin contact is modeled by coupling lug and pin displacements in the radial direction. Since the extent of the contact area is not known a priori, the problem is solved iteratively. An initial contact area is assumed, loads applied, and displacements and reactions forces in the lug and pin calculated. The forces that develop between coupled points on the lug and pin are then investigated. If the force at a given point is compressive, the lug and pin remain in contact at that point; if tensile, the two separate. The model then analyzes the new contact area, and the contact forces are again investigated. This process continues until the contact area stops changing.

The converged displacement field is then used to perform a laminate analysis on an element by element basis. For each element, the average strain in a given ply is calculated by integrating the strain field over the volume of that ply contained in the element, and the average strain at an interface is calculated by integrating over the interface area. These strains are then used to calculate average ply and interface stresses within the element. Either stress or strain

may then be used in an appropriate failure criteria to evaluate the integrity of the element.

Advantages of this approach over existing finite element models are 1) model geometry is defined in only two dimensions, 2) three dimensional stress and strain fields are used, 3) the effects of the laminate stacking sequence are included, 4) both in-plane and out-of-plane loads are included, and 5) ply and interface stresses and strains are calculated. Although existing methods have some of these advantages, no other approach has all of them.

In order to verify the analytical code developed, three lug lay-ups and two pin diameters were chosen (Figure 8). Each lug has a different through-the-thickness stiffness distribution, but all have the same average in-plane stiffness. The lug with the smaller pin diameter was sized to fail in bearing, and the lug with the larger pin diameter was sized to fail in shear.

Based on sensitivity study results, four elements through the thickness were used for strength prediction of lugs. A comparison of bearing strain distributions at 40 kips predicted by models consisting of one, two or four elements through-the-thickness is shown in Figure 9.

The lug specimens were tested as shown in Figure 10. Test results and associated predictions for the lugs are summarized in Figure 11. Failure prediction in the critical elements was based on using a modified Hashin criteria. The 1.75 inch diameter holes exhibited a tensile fiber failure at the net section while the 1.0 inch diameter showed permanent yielding around the hole prior to shear bearing failure. Good correlation between test and prediction was obtained. The initial bearing failure load was determined by using axial strain data from the rosettes located 0.5 inches away from the edge of the hole. The load versus strain curve in Figure 12 shows that axial strain decrease associated with material failure ahead of the pin. Typical bearing and net section failure modes can be seen in Figures 13 and 14 for the 1.0" and 1.75" diameter specimens, respectively.

Frame Elements

The Y-section frame elements, Figure 15, will be fabricated and tested against a T-section of contemporary design. Both sections will be coconsolidated to a typical skin laminate during fabrication.

The Y-section was chosen for its potential formability in a diaphragm forming process and for its lower peel stress components. The effect of changing the angle of the Y-section is also being investigated. Two-dimensional finite element models of the T- and Y-sections were created for the purpose of defining the boundary conditions to be used in testing.

The fastenerless moldline Y-frame attachment element design is structurally simple, allowing it to be diaphragm formed and coconsolidated. Transverse tension strength for semicrystalline thermoplastic composites has been found to be appreciably greater than comparable thermosets. This property is expected to enhance the peel strength and survivability of the frame element and will be verified by our planned tests.

Test loads for the Y-sections will be introduced through an internal mandrel (Figure 16). This method alleviates possible failures other than those desired and allows for later design of several frame attach possibilities. Possible frame attachments include: amorphous bonding, resistance joining, adhesive bonding, coconsolidation, and mechanical fastening.

SUBCOMPONENT TOOLING AND MANUFACTURING

Tooling concepts for each cover design/manufacturing concept is discussed. Internal geometry of the hat stiffeners was designed to be similar to allow mandrel tools to be interchangeable.

The fiber placement manufacturing process consists of placing inverted roll formed hat stiffeners into an aluminum fiber placement tool. Aluminum mandrels will be placed in the hat stiffeners to prevent skin deflection during the fiber placement process. Tooling conceptual design is illustrated in Figure 17. Retainers are utilized to hold the stiffeners and mandrels in place during processing. The hat is positioned in the tool as shown in Figure 18. The hat flange is offset slightly above the aluminum tool to allow for adhesive and the first ply. Also, a heat blanket will be embedded into the aluminum tool that supports the preformed thermoplastic composites stiffeners. The blanket will provide a greater degree of temperature control where required. Following fiber placement of the skin, the panel will be trimmed and retainers removed. The mandrels will then be removed and the part prepared for nondestructive testing.

The SDCC concept is unique in that there is but one diaphragm, and the IML pan and OML skin are consolidated and coconsolidated during the diaphragm forming process. The SDCC tooling concept is illustrated in Figure 19.

The greatest risk in diaphragm forming over hat mandrels is the chance for bridging. To minimize this risk, the manufacturing and tooling team members utilized lessons learned criteria to optimize hat height, cap width, and skin thickness. Hat spacing was maximized to increase ply surface area between mandrels. The increased surface area will increase the force exerted to form the ply pack and prevent bridging. In addition, the mandrel will be fabricated with a slight radius (Figure 20). The gap between the mandrel, OML skin, and IML pan will be filled with a predetermined amount of unidirectional tow. This fillet area has the highest probability for bridging; however, with the unidirectional fillet, the pressure will be equally distributed to facilitate a quality consolidation.

A vacuum ring and a neat film layer will aid in ply pack location. The IML ply pack will be contained between the aluminum diaphragm and a layer of neat film. A vacuum ring surrounds the IML ply pack and vacuum draws the aluminum diaphragm to the upper surface of the IML ply pack and the neat film to the lower surface of the IML ply pack. The IML ply pack is then positioned correctly above the tool prior to application of heat and pressure. The neat film is coconsolidated between the IML and OML ply packs during the press operation. This will permit accurate location of the IML ply pack and aid in prevention of wrinkles.

Concepts for the subcomponent tool include machined steel weldment, cast bulk ceramic, machined aluminum, and a metal arc sprayed tool. A metal arc sprayed tool which can accommodate integral heating, faster cycle times, and low tool cost for production-type environments shows high potential.

ELEMENT TOOLING AND MANUFACTURING

Lug Elements

Tooling for the lug specimens consisted of simple project plates with steel dams positioned to allow for expansion during consolidation. The lug geometries and lay-ups that will be used were previously described in Figure 8.

The lugs were fabricated from AS-4/PEEK unidirectional tape. Eighteen 30" x 16" sublaminate panels of four different 30 ply lay-ups were consolidated in a hydraulic press. Six sublaminates were then stacked to form the three different 180 ply stacking sequences. The three stacking sequences were co-consolidated in the autoclave. The lug specimens were water jet cut from the panels and the holes reamed to final dimensions. Excellent consolidation was achieved in all lug specimens as evidenced by ultrasonic and photomicrographic inspections.

SDCC and Y-Frame Elements

An SDCC element verification tool (Figure 21) was developed which can incorporate either two hat mandrels or a single triangular mandrel to fabricate the Y-section frame elements. The hat dimension, spacing, height and width simulate the subcomponent design. The hat stiffener mandrels, located by pins, float on the unconsolidated skin. The inner skin is then formed over the mandrels in a press operation. The aluminum tools are readily extracted following forming.

To focus on the critical process variables and not on geometric complexities, element forming trials on the verification tool commenced with the Y-frame elements and will then proceed to the 2-hat section element. Scale-up is a very significant concern and is being considered in all the fabrication development activities.

Forming trials on the single "Y" configuration used one diaphragm to consolidate the upper ply pack with the lower plies. Initially full pressure (150 psi) was applied after the melt temperature of the ITX was reached but was maintained for only 5 minutes at which point the diaphragm ruptured. In spite of the short hold time the pressure was sufficient to fully consolidate the flat areas of the part and to form the material over the mandrel. The upper ply pack conformed to the mandrel surface very nicely, but the diaphragm rupture caused the outer ply to lift and bridge across the mandrel/skin intersection. The other plies remained in the formed condition, nesting closely to the mandrel, and showed excellent definition at the interface between stiffener web and lower skin.

Forming was next done below melt temperature because of anticipated problems where the two packs met each other beyond the stiffener area. For the next trial full melt temperature was achieved before pressurizing. Other changes to the setup included lengthening the mandrels to rest next to the ramp surfaces and widening the upper ply pack so it extended out to the ramp surfaces in all directions. This change required notches to be cut along the edge of the ply pack to prevent buckling and rupture of the diaphragm. Kapton tape was used to cover the notches for additional protection.

The next forming runs were performed with the noted changes and the diaphragm survived well up through 150 psi. Since the plies were above melt temperature, good consolidation was achieved between the upper and lower packs. The rupture occurred along the edge of the mandrel in a notch location that allowed the film to over elongate and burst. A large percent of the plies remained formed to the mandrel surface along its base. Only one ply lifted and bridged away from the radius area of the formed plies (Figure 22). The inside of the stiffener shape revealed very good contact between the plies being formed and the base of the mandrel even with loss of the diaphragm. Photomicrographs of the area show that the upper plies dragged the lower plies in toward the mandrel and formed wrinkles in the lower skin.

In an attempt to alleviate dragging of the base ply pack, the upper ply of the base pack was extended to run under the ramp areas of the tool. This change would maintain pressure on the top ply to allow slippage of the two ply packs without wrinkling. Also, a fiber glass cloth (picture frame), was placed around the ramp areas and over the mandrel to cover any areas that could potentially allow the diaphragm to rupture. During this run the diaphragm ruptured in a gap between the ramp and forming box causing incomplete forming of the element. However, less ply slippage was noted.

Due to the frequency of rupture of the UPILEX diaphragms, an aluminum (SUPRAL) diaphragm was selected for further trials. The aluminum diaphragm offers greater elongation capabilities not only at processing temperatures but also at temperatures below the melt temperature of the PEEK resin.

During the first run with an aluminum diaphragm, the pressure was applied at 550°F, (below the melt temperature of the thermoplastic resin). Applying the pressure at this low temperature allowed the lower plies to slip prior to a viscosity change of the resin. During this fabrication attempt, the top ply of the lower ply pack was extended beneath the forming ramps in an attempt to "lock" the ply in place, thus avoiding wrinkles. After applying pressure (120 psi) at 550°F, the temperature was increased to 750°F and held for 30 minutes.

The result was a stiffened panel with good surface quality but with bridging in the radius. NDT results revealed a porosity free part in the flat areas. However, photomicrographs revealed the lower ply pack wrinkled. Since the upper ply of the lower ply pack wrinkled and the ends were contained beneath the forming ramps, the ply obviously split between the fibers of this outer 45° ply.

Following review of the results of the run, two changes to the manufacturing process were identified to alleviate the wrinkling problem in the next run. The next attempt will incorporate a neat resin film between the two ply packs

to serve as a lubricant. This will reduce frictional forces to allow the two contacting plies to slip past each other. Another potential solution is to change the two contacting plies from 45 degrees to 90 degree orientations. This will increase the strength in the direction of slippage and reduce friction.

Blade Frame Elements

Using two aluminum block details a blade panel was hand laminated by bending and edge tacking each of seven plies with a soldering iron (Figure 23). The fillet was filled with thin strips (.30" to .90") of ITX unidirectional tape using a sharp cone tip on the soldering iron, Figure 24. A flat skin was preconsolidated and a strip grit blasted across the center where the blade attached (Figure 25). The two angles with fillet in place were inverted onto this skin, Figure 26, and vacuumed bagged to a project plate. There was a released UPILEX film between the angle plies (web) and the aluminum details. Upon consolidation (Figure 27) this configuration did not show acceptable c-scan results. The web area had many depressions in it that appeared to be oriented along the second ply down from the surface, i.e., normal to the surface ply fiber direction.

Outgassing from the release coated UPILEX and the lack of ears on the vacuum bag at the base (which may have prevented sliding of the blocks) were identified as probable causes for the poor consolidation. As such, a second blade was fabricated with no UPILEX on the tool details and with extensive ear folds in the vacuum bag. Nondestructive inspection of the second blade revealed porosity in the radius areas. Although the part quality was improved over the first blade, it was not the level desired. After a careful review of the part it was evident one of the tool details had slightly rotated during consolidation.

The consolidation tools are presently being modified to permit a positive control of the details. A trimetric view of the modification is shown in Figure 28. Keyways will be milled into the ends of the web details and fit to keys in the end plates. This modification will maintain the movement of the detail in the direction desired, thus maintaining constant and equal pressure across the part surfaces. In addition, an upper slotted plate will maintain minimum differential vertical displacement between the tooling blocks for the back-to-back L-sections which comprise the T-section.

CONCLUSIONS

Based on work to date, the following conclusions have been made:

- Selection of the upper cover allows for the demonstration of two promising cost-effective manufacturing approaches, fiber placement and single diaphragm/co-consolidation, which have applications in a majority of the remaining generic fuselage section.

- The producibility analysis indicated that the selected manufacturing approaches show potential for low cost fabrication of the upper cover. The accuracy of the analysis will be verified during subcomponent fabrication.

- The use of an aluminum diaphragm during SDCC verification trials prevented diaphragm rupture due to increased durability and elongation properties compared to available polymeric films.

- During SDCC pressure can be applied below resin melt temperature without fear of diaphragm rupture since aluminum diaphragms provide sufficient elongation at those temperatures.

- Based on blade fabrication attempts, it is anticipated that control of the tooling movement through selected keyways will guarantee cap and web thicknesses and supply adequate pressure in the fillet area.

- Quality, thick (1 in.) panels (for lug elements) can be successfully fabricated.

- Abrasive waterjet cutting can be used to efficiently machine thick panels.

- A lug analysis program capable of investigating through-the-thickness effects showed good correlation to experimental results.

REFERENCES

1. Hoffman, P.L.R. and Gibler, J.A., "Design for Manufacturing, Producibility Issues for Thermoplastic Composites," presented at SAMPE Spring Meeting, Anaheim, CA., April 4, 1990.

2. Wilkins, D.J., "Anisotropic Curved Panel Analysis," Report FZM-5567, Air Force Contract No. F33615-69-C-1494, May 1973.

3. Goering, J., "Initial Impact Damage of Composites," Material Science Corporation Report MSC TFR 1801/1207, March 1987.

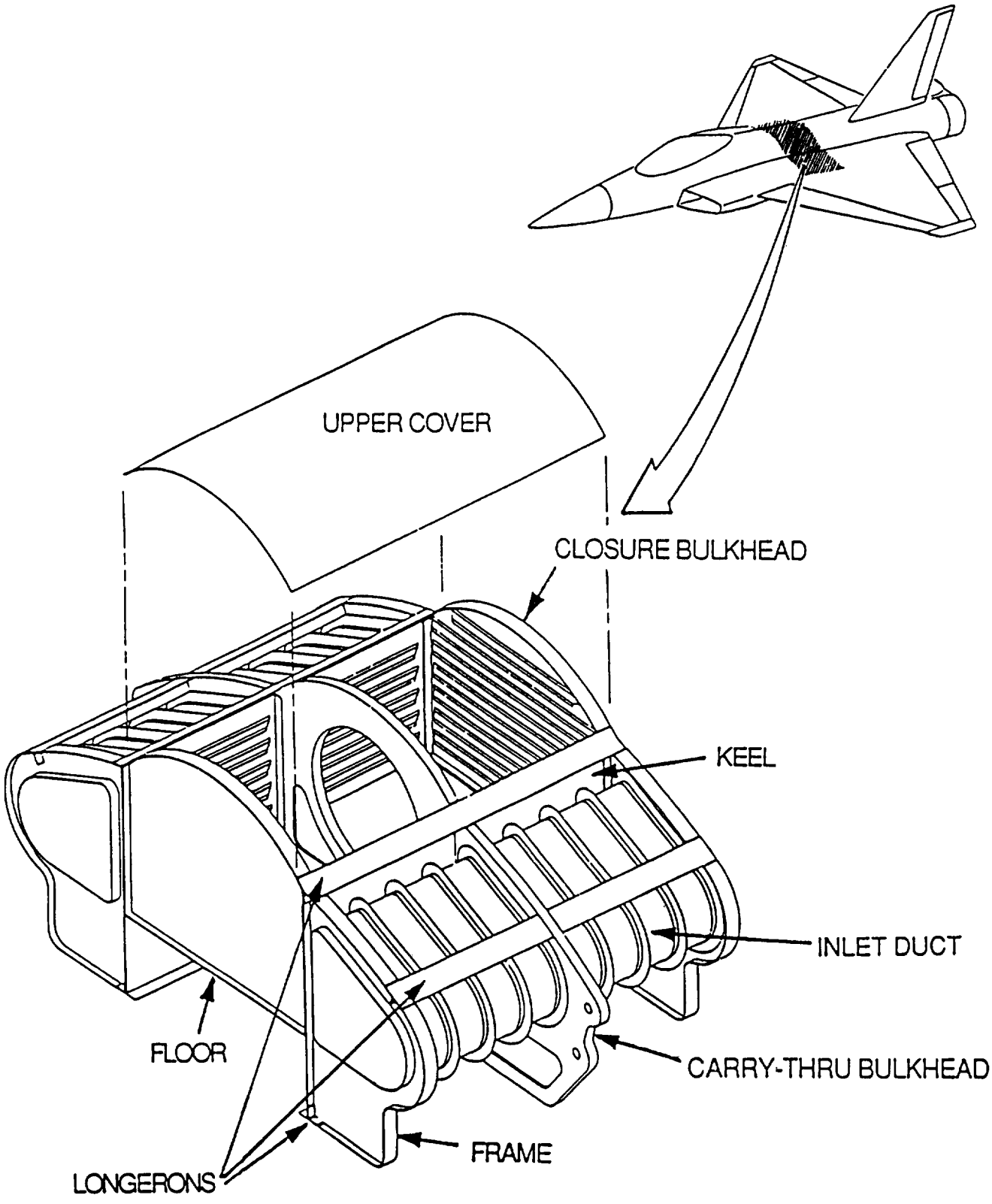

Figure 1 Generic Fuselage Section

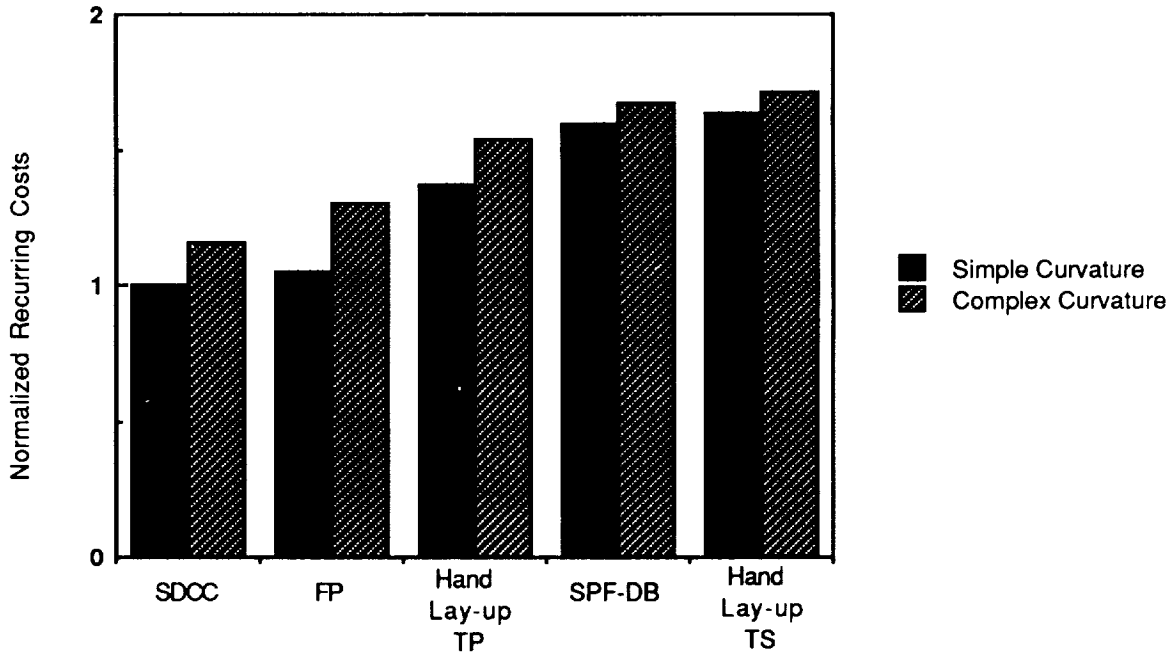

Figure 2 Recurring Cost Comparisons

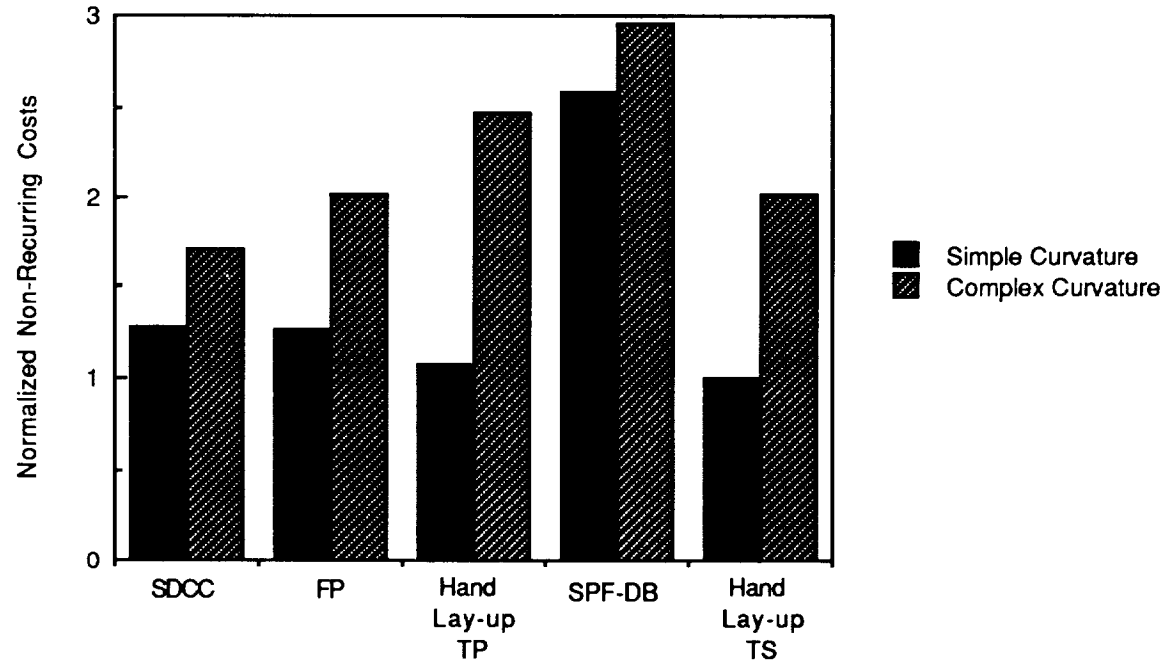

Figure 3 Non-Recurring Cost Comparisons

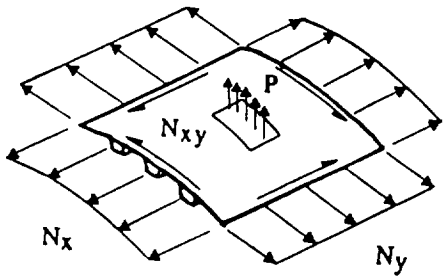

Phase A Subcomponent

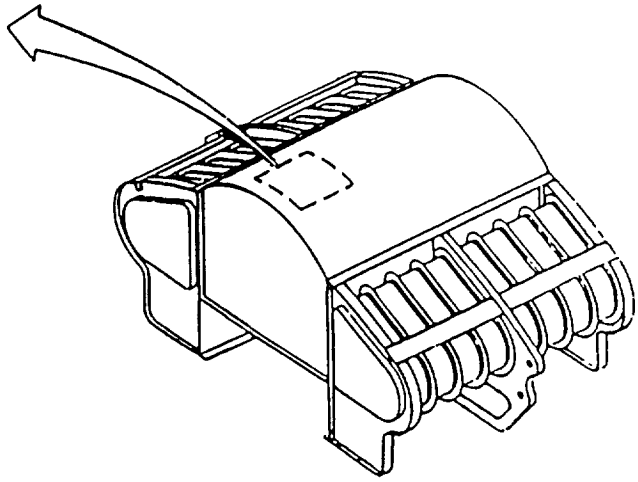

Ultimate Loads

Condition	Nx (lb/in)	Ny (lb/in)	Nxy (lb/in)	P (psi)
SSPU, 0.95 MACH, SL, 9.0 g	2500	±100	0	1.0
SSPD, 0.95 MACH, SL, -3.0 g	-800	±100	0	5.0
RPO, 0.95 MACH, SL, 7.2 g	2000	±100	±500	5.0
Fuel System Over Pressure Malfunction	0	0	0	22.0

Figure 4 Subcomponent Designed for Actual Flight Loads

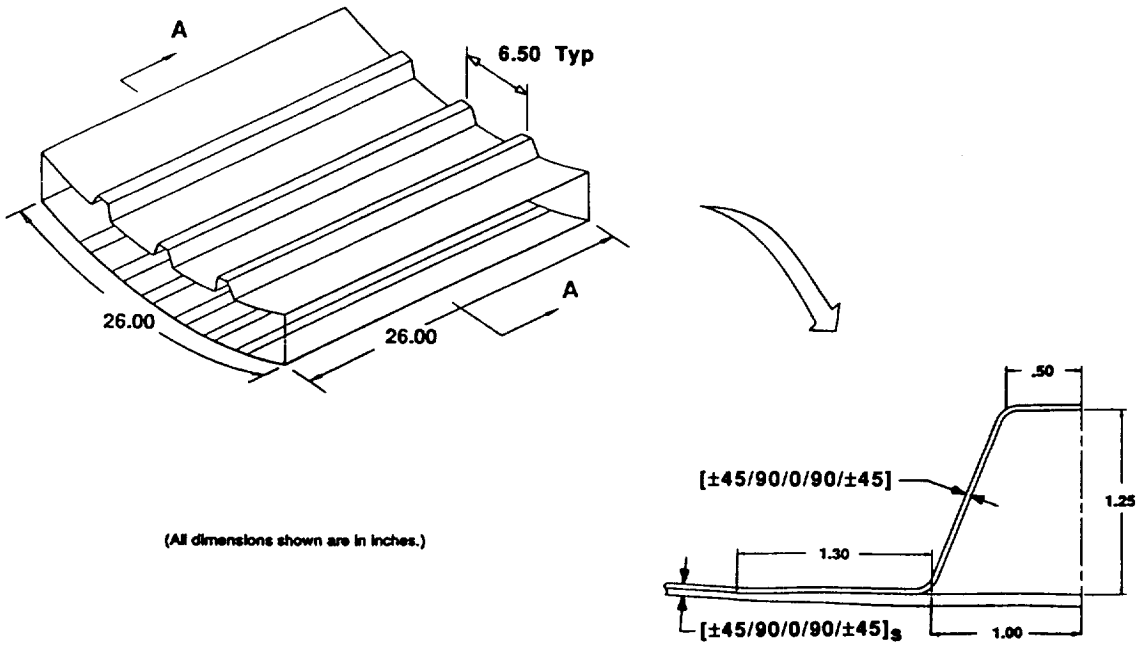

Figure 5 SDCC Subcomponent Configuration

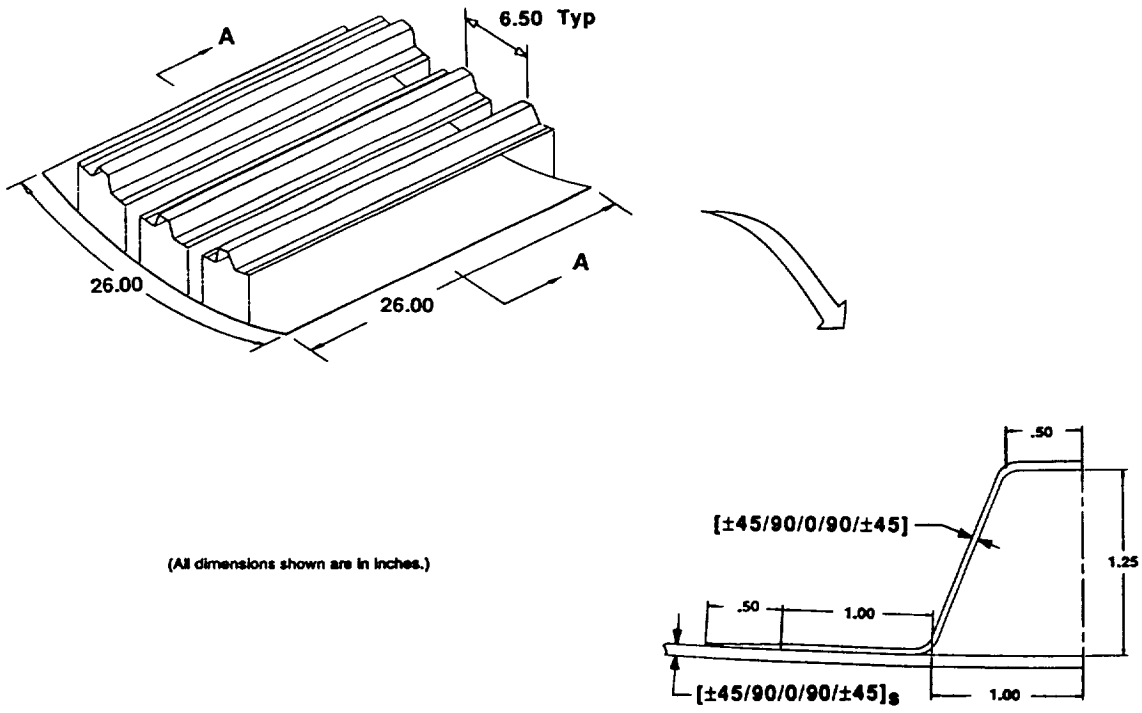

Figure 6 Fiber Placement Subcomponent Configuration

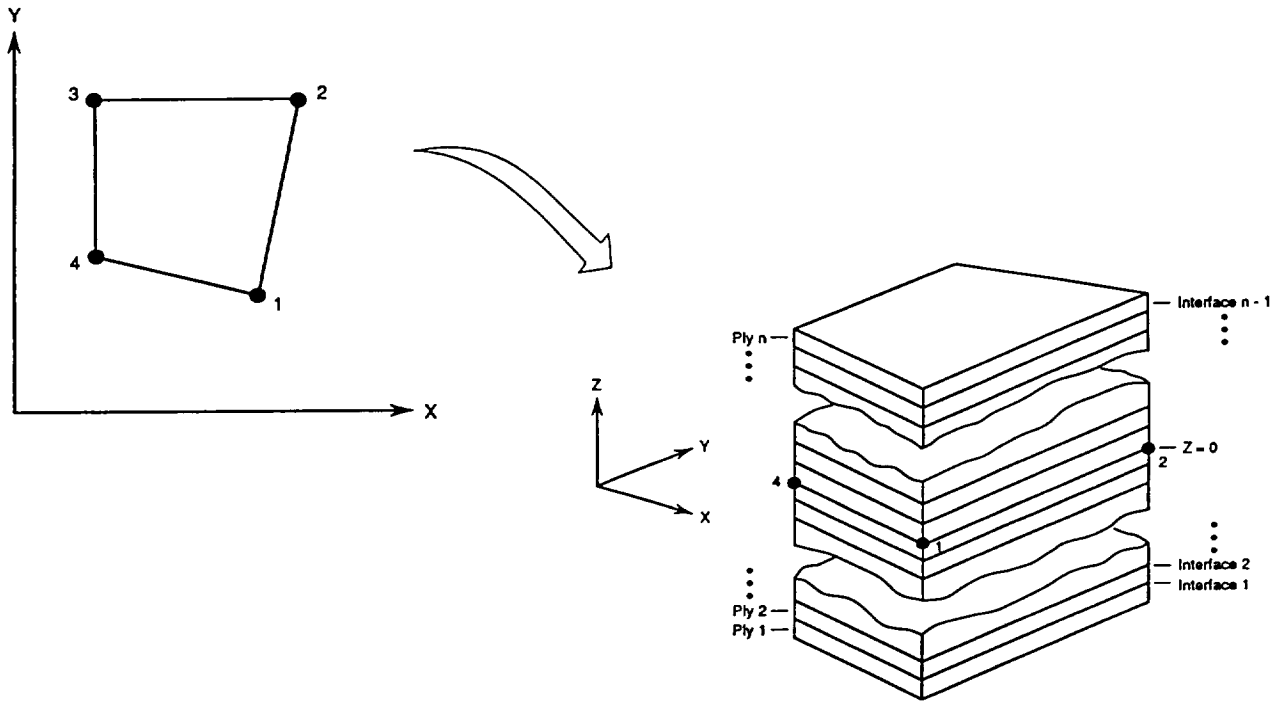

Figure 7 Subparametric Laminated Solid Element

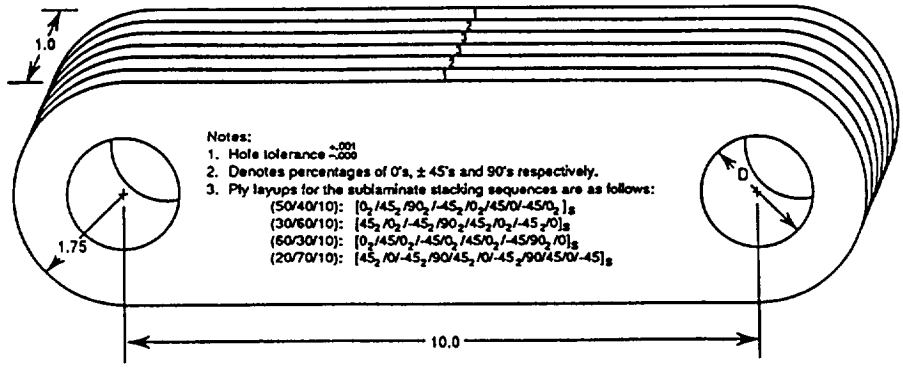

Lug Specimens	Quantity Each	Hole Diameter[1]	Subliminate Stacking Distribution[2,3]		
			Subliminate 1	Subliminate 2	Subliminate 3
Static 1	4	1.00	(50/40/10)	(50/40/10)	(50/40/10)
Static 2	4	1.00	(50/40/10)	(30/60/10)	(60/30/10)
Static 3	4	1.00	(60/30/10)	(50/40/10)	(20/70/10)
Static 4	4	1.75	(50/40/10)	(50/40/10)	(50/40/10)
Static 5	4	1.75	(50/40/10)	(30/60/10)	(60/30/10)
Static 6	4	1.75	(60/30/10)	(50/40/10)	(20/70/10)

Figure 8 Lug Element Tests to Verify Analytical Methodology

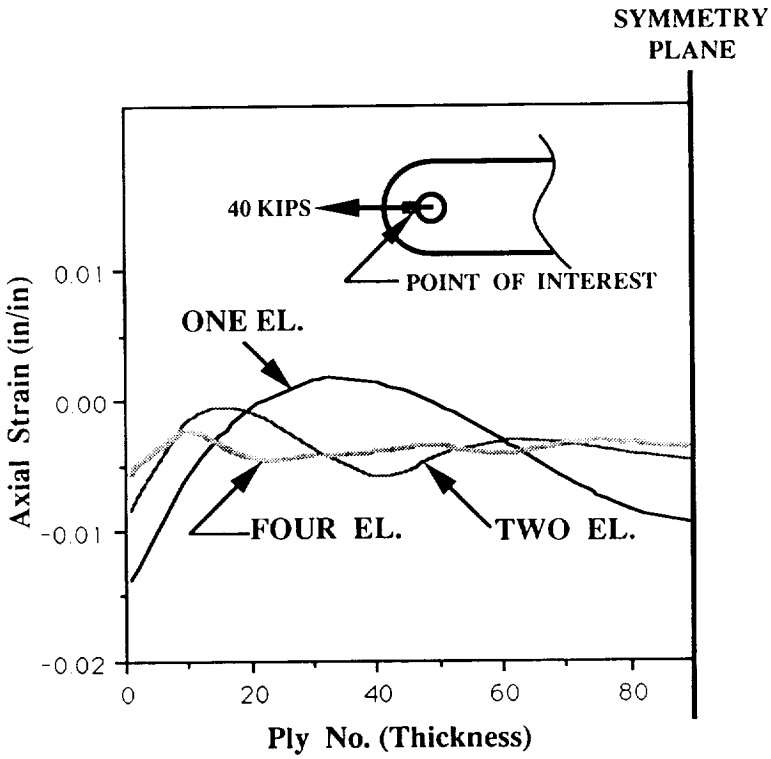

Figure 9 Convergence Study Indicates Four Elements Through-the-Thickness are Necessary

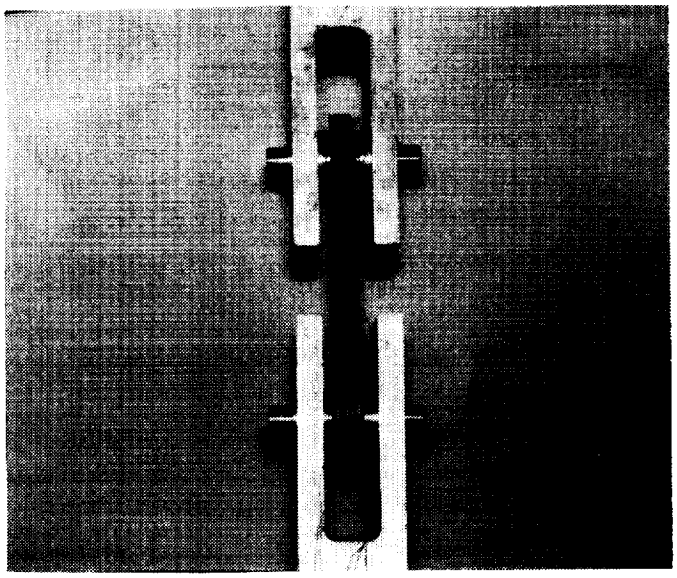

Figure 10 Lug Element Under Test

LUG Specimen	Quantity Each	Hole Dia. (inches)	Pred. Failure Load (kips)	Test Results (kips)
# 1	4	1.0	64.2	60.1 (76.7) *
# 2	3	1.0	65.9	62.3 (74.3) *
# 3	4	1.0	57.3	62.2 (74.7) *
# 4	4	1.75	66.9	69.3 **
# 5	4	1.75	66.5	68.7 **
# 6	4	1.75	61.5	66.8 **

* Initial Bearing Failure Load (Final Failure Load)

** Failure Load

Figure 11 Lug Test Results Showed Good Agreement to Predictions

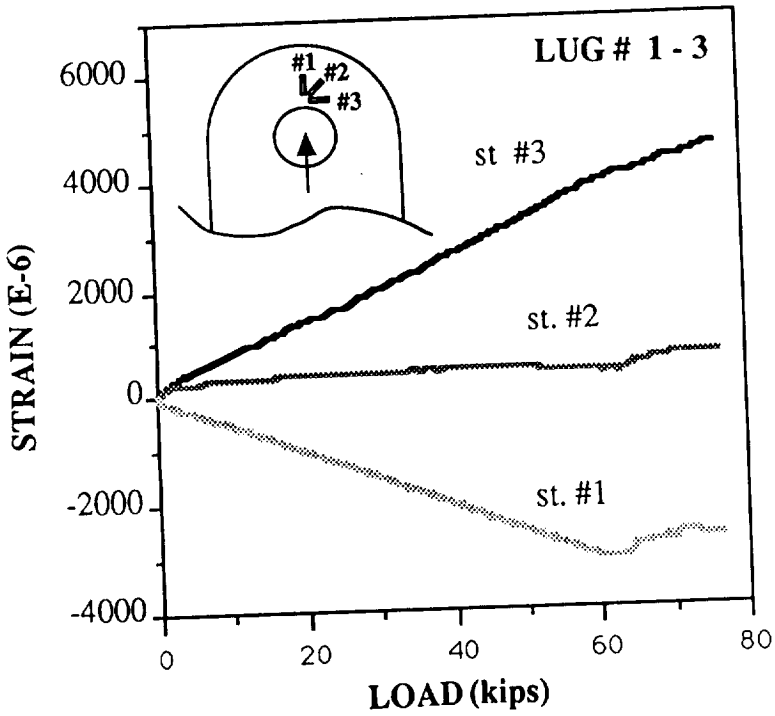

Figure 12 Strain Data Indicates Point of Bearing Failure

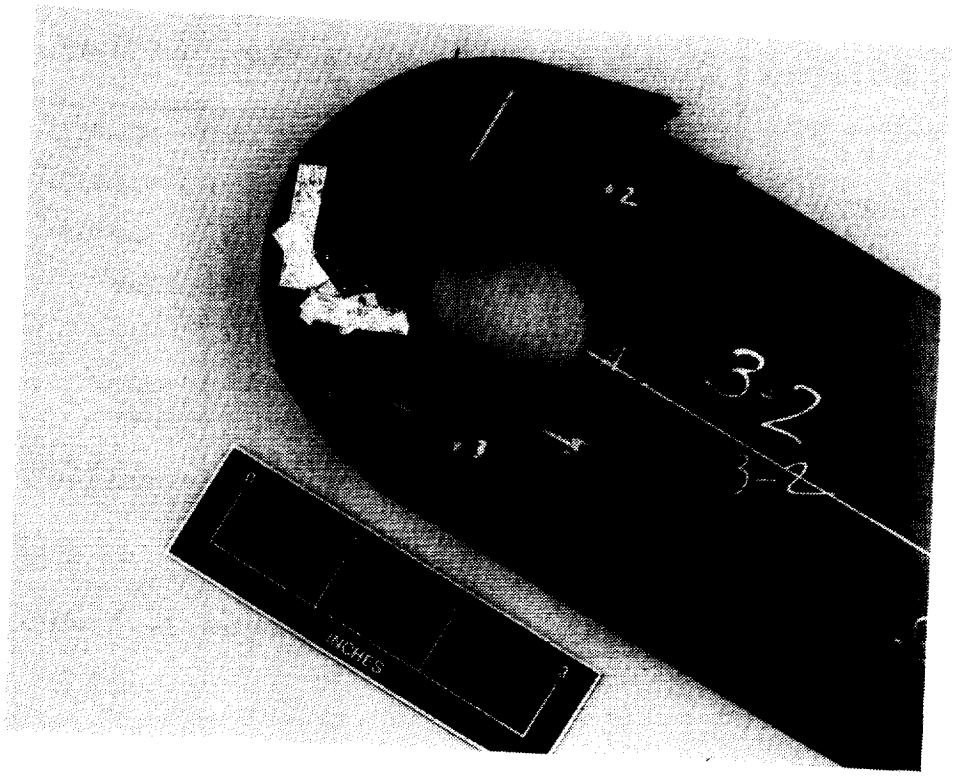

Figure 13 Typical Lug Bearing Failure

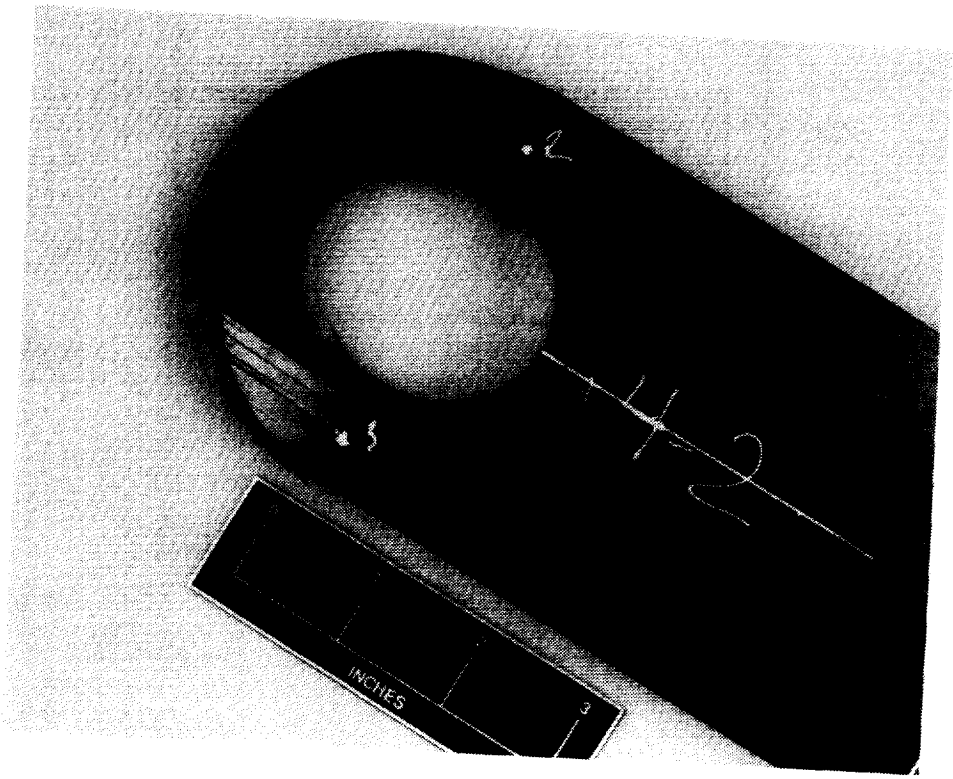

Figure 14 Typical Lug Net Section Failure

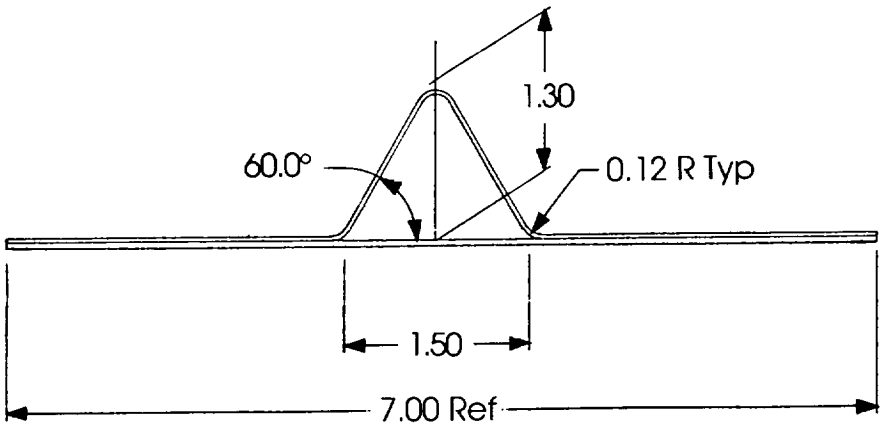

60° Y-Frame Specimen

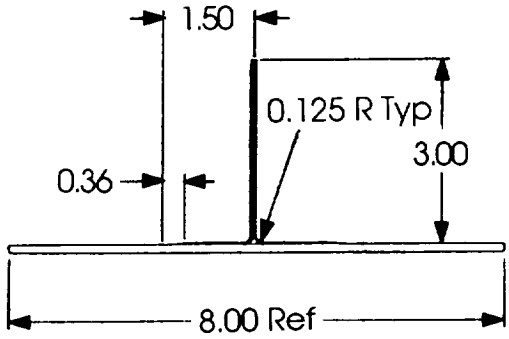

Blade Specimen

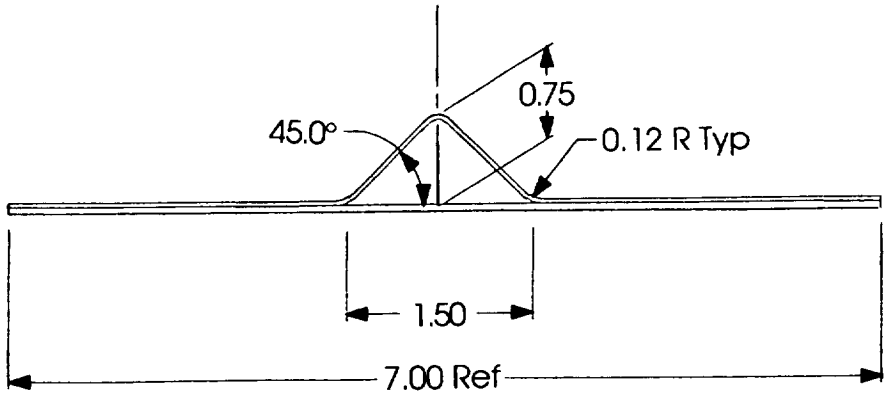

45° Y-Frame Specimen

Figure 15 Frame Element Test Specimens Will Determine Viability of Fastenerless Moldline Designs

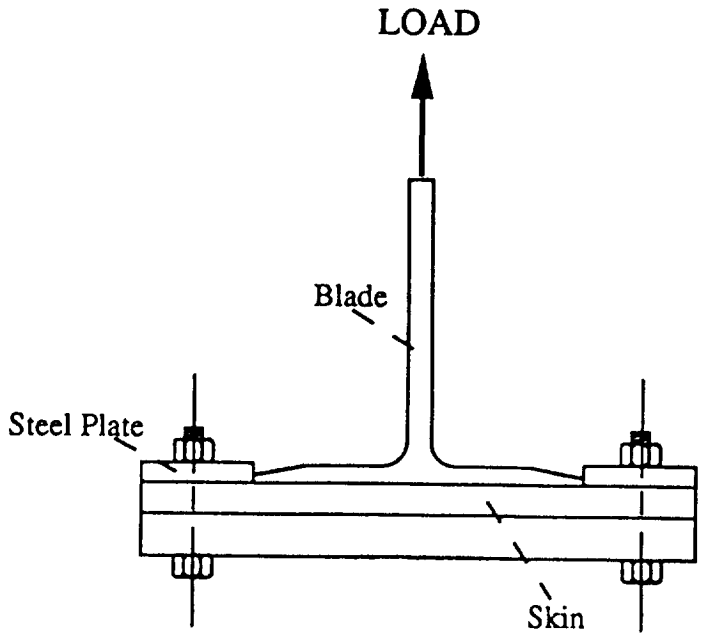

Frame Configuration	Static	
	RTA	ETW*
Blade	3	3
Y(α = 45)	3	3
Y(α = 60)	3	3

* 255° F

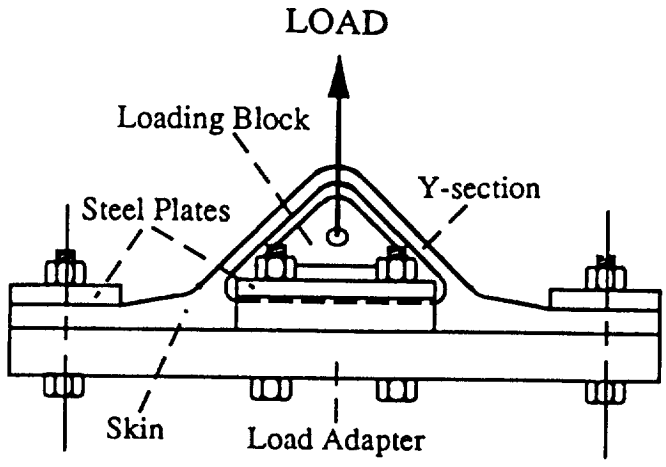

Figure 16 Pull-off Test Method Will Ensure Failure In Critical Regions

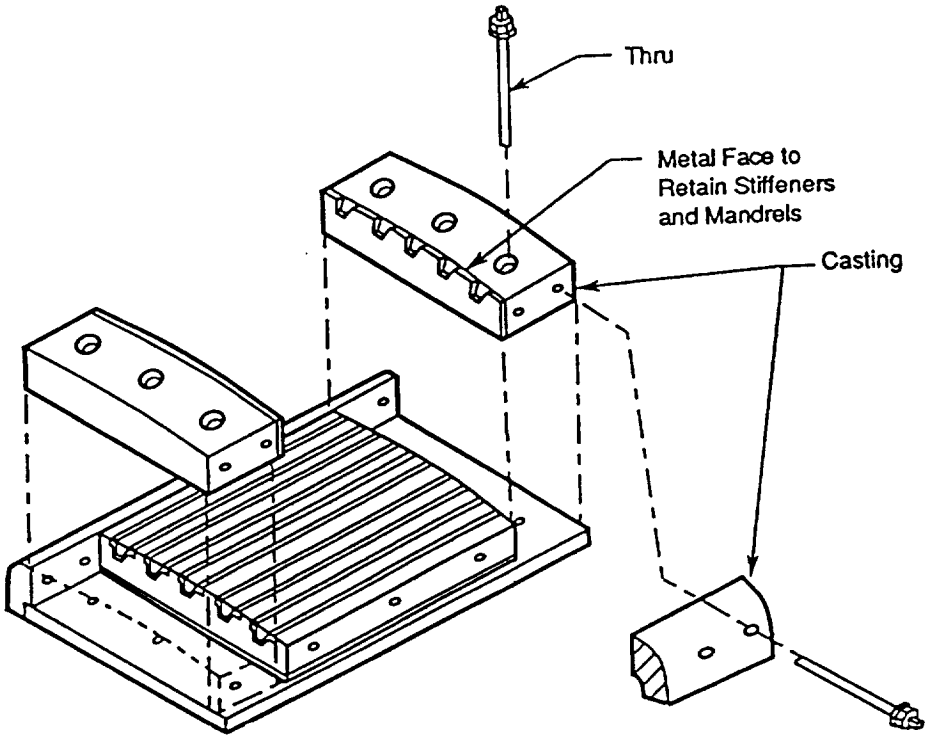

Figure 17 Fiber Placement Tooling Concept

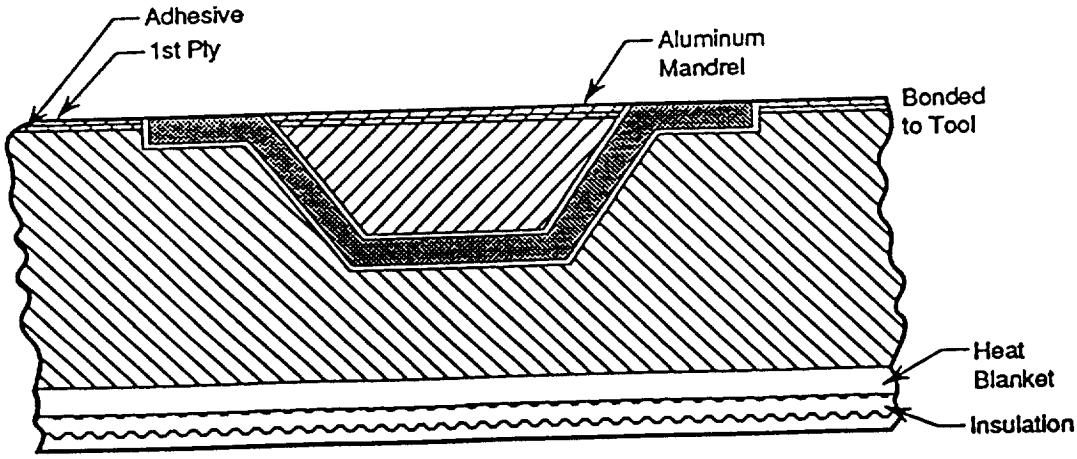

Figure 18 Hat Stiffener Embedded In Fiber Placement Tool

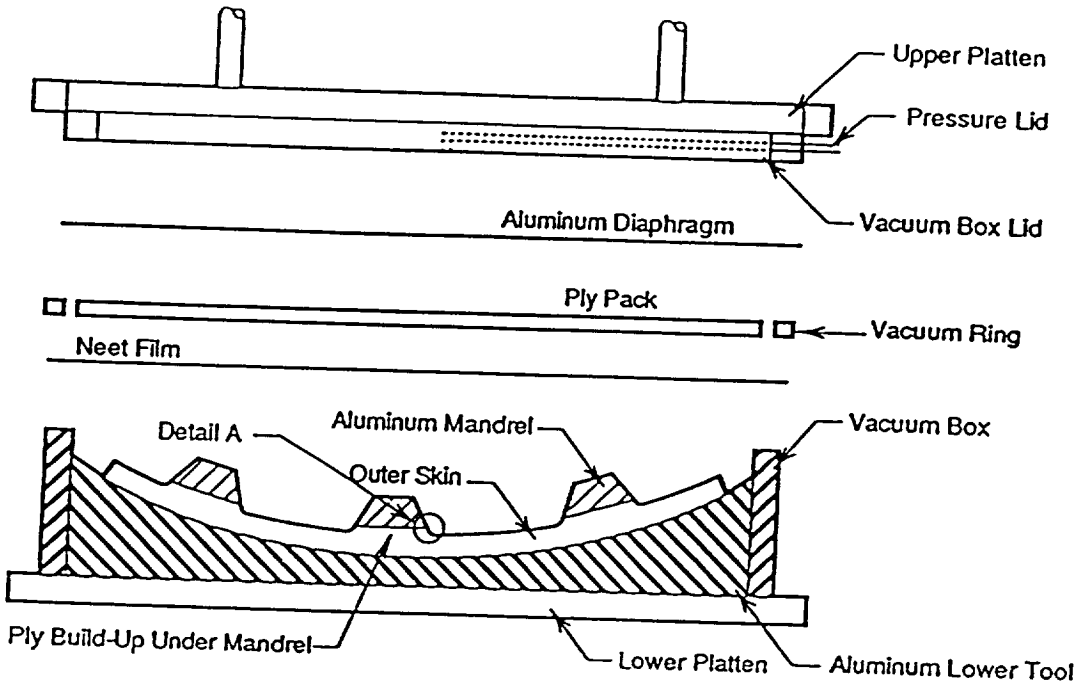

Figure 19 SDCC Tooling Concept

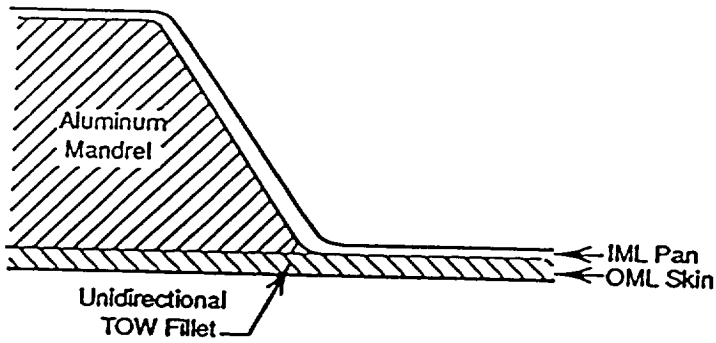

Figure 20 Unidirection Tow Used In Fillet Area to Assure Part Quality

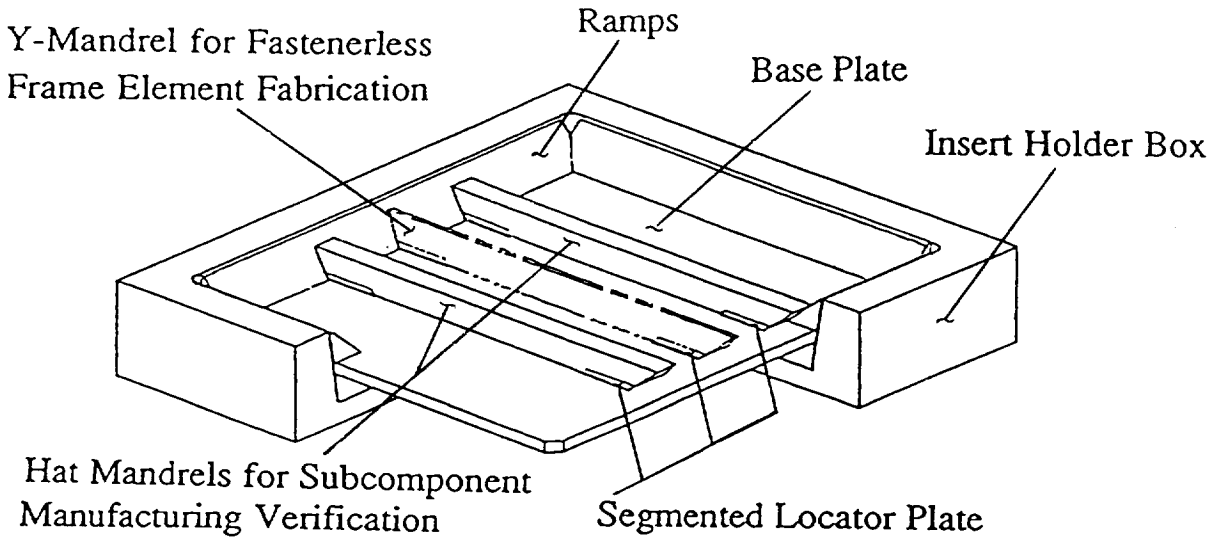

Figure 21 SDCC Element Tool

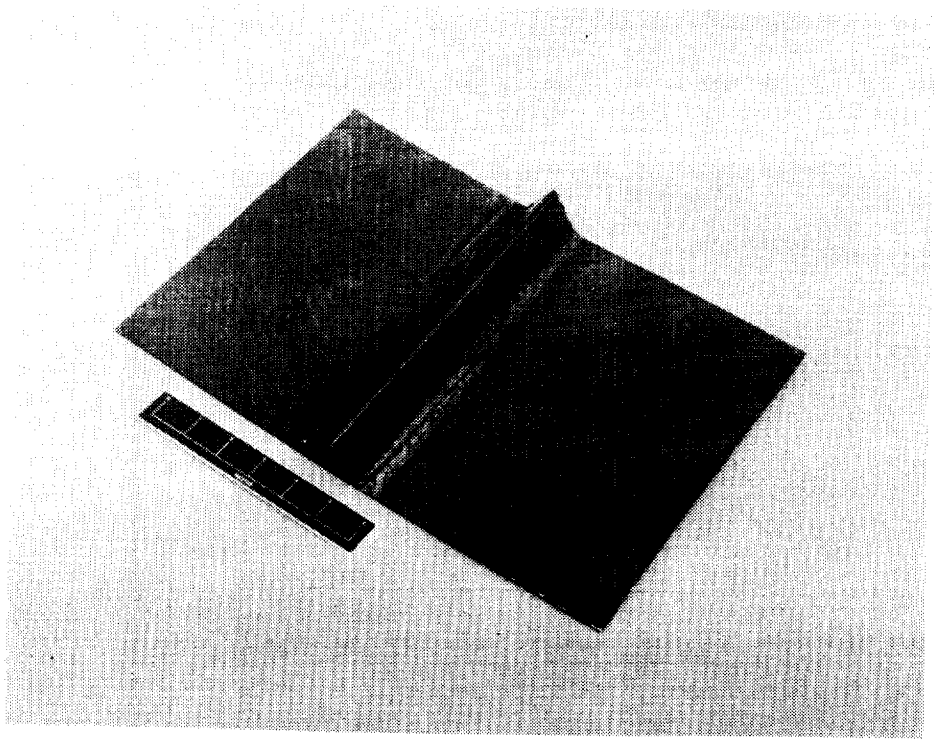

Figure 22 Initial Y-Frame Element Experienced Bridging in Radius

Figure 23 Blade L-Section Plies Hand Laid On Tooling Blocks

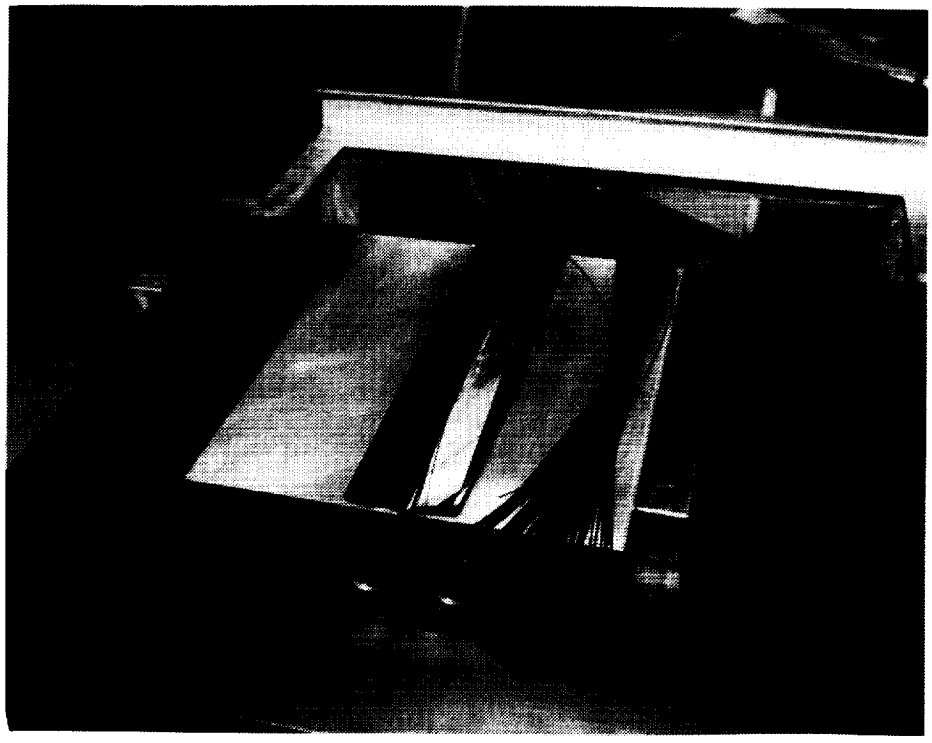

Figure 24 Tow Material Was Placed In Fillet Area

Figure 25 Base Plies Consolidated, Separated and Grit Blasted Prior To Assembly

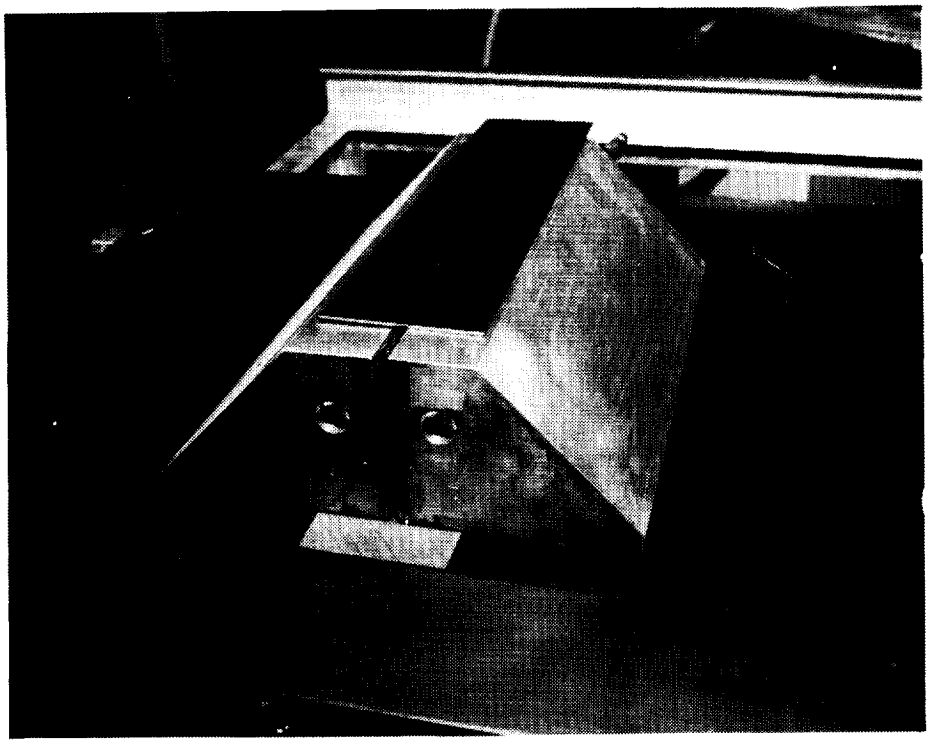

Figure 26 Assembly Prior To Autoclave Consolidation

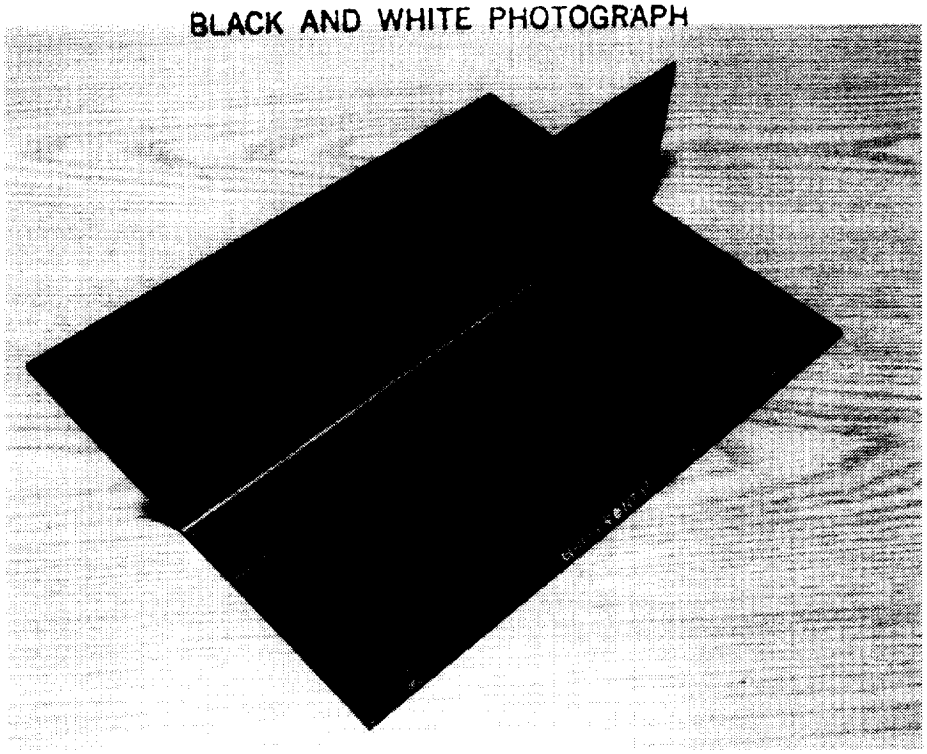

Figure 27 Intra Blade Elements Contained Porosity In Radius Due To Insufficient Pressure

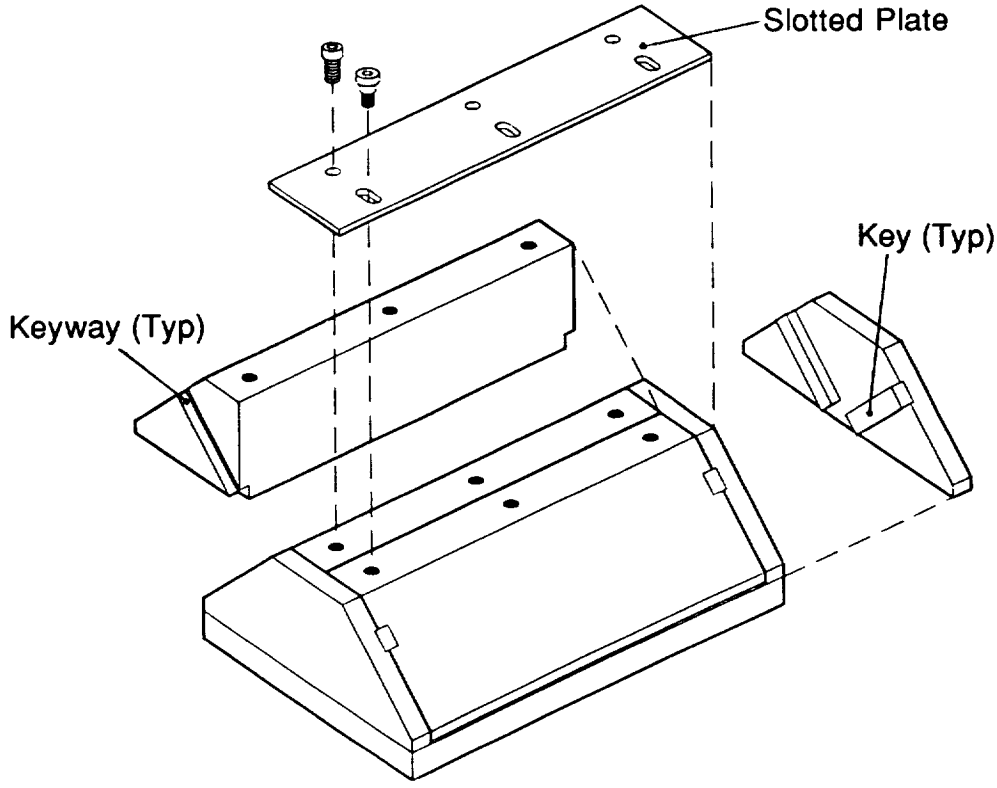

Figure 28 Modifications To Blade Element Tooling To Ensure Proper Pressure In Radius